INSTITUTE OF PHYSICS PUBLISHING NANOTECHNOLOGY
Nanotechnology **18** (2007) 044005 (8pp) doi:10.1088/0957-4484/18/4/044005

Electrical characterization of 7 nm long conjugated molecular wires: experimental and theoretical studies

Changsheng Wang[1], Andrei S Batsanov[1], Martin R Bryce[1], Geoffrey J Ashwell[2], Barbara Urasinska[2], Iain Grace[3] and Colin J Lambert[3]

[1] Department of Chemistry, Durham University, Durham DH1 3LE, UK
[2] The Nanomaterials Group, Cranfield University, Cranfield MK43 0AL, UK
[3] Department of Physics, Lancaster University, Lancaster LA1 4YB, UK

E-mail: m.r.bryce@durham.ac.uk, g.j.ashwell@cranfield.ac.uk and c.lambert@lancaster.ac.uk

Received 28 July 2006
Published 12 December 2006
Online at stacks.iop.org/Nano/18/044005

Abstract
This article describes arylene–ethynylene molecular wires with 7 nm long backbones and thiolated termini. Cyclic voltammetric studies in solution reveal that the reduction waves of the fluorene, 9-[(4-pyridyl)methylene]fluorene and 9-[di(4-pyridyl)methylene]fluorene units which are embedded in the conjugated π-systems endow these wires with n-doping characteristics. An x-ray crystal structure investigation of 2,7-diiodo-9-[bis(4-pyridinium)methylene]fluorene bis(tetrafluoroborate) **8** established that protonation occurs on both nitrogens of this unit. Self-assembled monolayers of the 7 nm wire **2** on gold substrates exhibit symmetrical current–voltage (I–V) characteristics when contacted by a gold scanning transmission microscope (STM) tip. The dipyridyl functionality of **2** served to obtain a rectifying junction in which the diprotonated cationic wire is the electron accepting component in combination with an adjacent anionic phthalocyanine as the electron-donating layer. This ionic Au–$\mathbf{2}H_2^{2+}[CuPc(SO_3^-)_4(Na^+)_n]_{2/(4-n)}$ bilayer assembly exhibits rectification with current ratios of 15–50 at ± 1 V. This dramatic change in I–V characteristics upon simple chemical manipulation proves that the conductivity is a property of the wire molecules **2** in the junction. *Ab initio* calculations suggest that the molecular wires possess useful structural features which allow the conductance of the molecule to be altered by changing the properties of the side groups attached to the fluorene units.

1. Introduction

It is widely recognized that the microelectronics industry is rapidly approaching an intrinsic miniaturization limit for silicon devices [1]. The emerging science of molecular-scale and nanoscale electronics embraces very different concepts from traditional inorganic electronics [2][4]. Chemical synthesis enables fine tuning of molecular structures and highest occupied molecular orbital and lowest unoccupied molecular orbital (HOMO–LUMO) levels for nanometre-sized organic molecules which can be functionalized for interconnecting into electronic circuits using techniques such as self-assembly at metal or semiconductor surfaces [3–7].

In this context molecular wires which facilitate intramolecular electron- or charge-transport from one site to another, usually under the control of an external electrical, electrochemical or photonic stimulus, are at the forefront of attention [8, 9]. New fabrication methods and probes

[4] The terminology 'molecular electronics' is often used very loosely in the literature. In this book two sub-categories were proposed, namely 'molecular materials for electronics' which is relevant for bulk applications, and 'molecular-scale electronics' for single molecule applications.

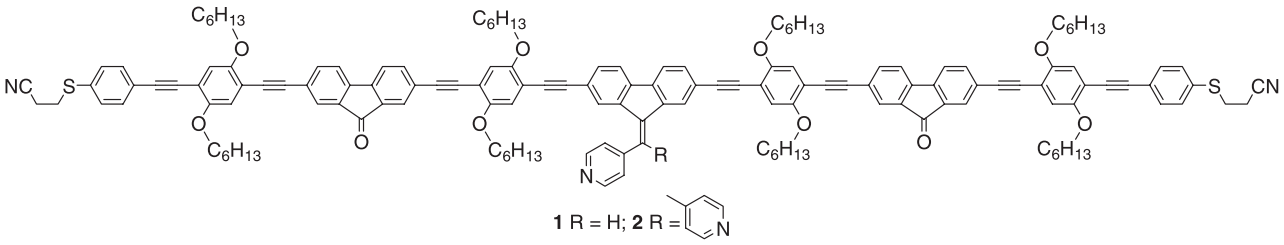

Figure 1. Molecular structures of the 7 nm wires **1** and **2** with terminal thiols protected as cyanoethyl derivatives.

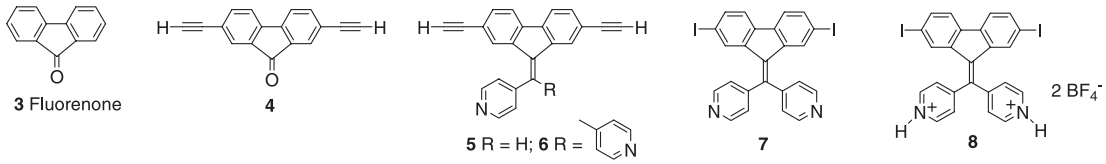

Figure 2. Molecular structures of model compounds **3**–**8** used in this study.

enable the molecular wires to be connected in a controlled manner into hybrid organic/semiconductor device architectures, thereby paving the way for studies of single-molecule devices [10–14]. For the covalent attachment of wire molecules onto metal surfaces, thiols (or protected thiols) are the most widely used terminal groups [15–18].

2. Design features of the molecular wires

Ethynylated aromatic systems, with the generic structure (aryl–C≡C−)$_n$, are π-conjugated systems with rod-like backbones which are available in incremental lengths from about 1 to 10 nm by iterative palladium-mediated Sonogashira strategies [19–22]. An attraction of these arylene–ethynylene motifs as molecular wires in metal–molecule–metal configurations is that they are more rigid π-systems and lack cis/trans isomerism, compared to their arylene-vinylene counterparts (aryl–CH=CH−)$_n$. However, the barrier to rotation around the aryl–ethynyl bond in (aryl–C≡C−)$_n$ wires is very low (about 1 kcal mol^{-1}) so although coplanar orientations (dihedral angles ±10°) of the arylene rings are often observed in the crystalline state (sometimes stabilized by intermolecular π-stacking interactions), their structures in solution or in molecular junctions may be considerably less well ordered [23]. The electrical properties of short thiol-terminated oligo(phenylene-ethynylene) oligomers (typically about 2 nm length) have been explored in various device architectures [18, 24–27]. More extended molecular systems have received considerably less attention. In this work we focus on arylene–ethynylene oligomers **1** and **2** (especially the latter) which possess the following key design features:

- the conjugated molecular backbones (i.e. the intramolecular S · · · S distances) are about 7 nm in length
- the phenyl rings possess hexyloxy side-chains to ensure good solubility in organic solvents
- the terminal thiol groups for chemisorption are cyanoethyl protected
- the oligomers are n-dopable due to the 9-fluorenone units and the central 9-[(4-pyridyl)methylene]fluorene (compound **1**) and 9-[di(4-pyridyl)methylene]fluorene moieties (compound **2**)
- protonation of the pendant pyridyl units can be readily achieved to produce a strongly electron-accepting cationic wire and a bilayer junction.

Table 1. Reduction peak potentials of compounds **1**–**6** (Note: For experimental conditions see the experimental section 8.2; (rev) and (irrev) denote electrochemically reversible and irreversible waves, respectively.)

Compound	E_{red} (V)
1	−1.49 (irr), −2.17 (irr), −2.42 (irr)
1-HCl	−0.88 (irr), −1.50 (rev), −2.19 (irr)
2	−1.51 (rev), −2.12 (irr), −2.41 (irr)
2-HBF$_4$	−0.91 (irr), −1.39 (irr), −1.75 (irr) −2.13 (irr)
3	−1.74 (rev)
4	−1.51 (rev), −2.25 (rev)
5	−1.75 (irr), −2.12 (irr)
5-HCl	−1.12 (irr), −1.69 (irr), −2.46 (irr)
6	−1.53 (rev), 1.70 (rev)
6-HCl	−0.89 (irr), −1.48 (rev), −1.60 (rev), −2.46 (irr)

The synthesis of the wires **1** and **2** has been described previously [28]. The molecular structures of **1** and **2** and relevant model compounds are shown in figures 1 and 2, respectively.

3. Molecular properties of the wires

3.1. Solution electrochemistry

The redox chemistry of the wires **1** and **2** and key building blocks **3**–**6** in solution was studied by cyclic voltammetry (CV), and the data are presented in table 1 and figures 3 and 4. The fluorenone units endow these compounds with n-doping characteristics, as seen by the reversible formation of the radical anion **3** at E_{red} − 1.74 V (versus Ag/Ag$^+$). It is evident from a comparison of fluorenone **3** and compound **4** (figure 3) that extending the conjugation with ethynyl substituents increases the electron affinity. The neutral → radical anion peak was positively shifted by 230 mV; a second

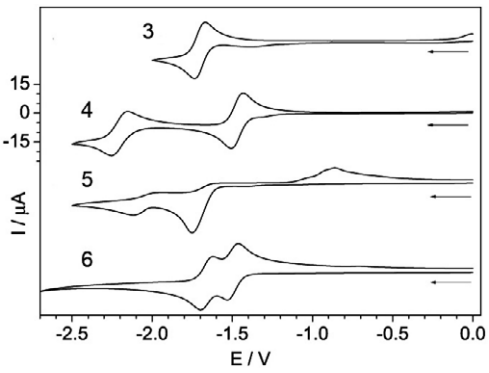

Figure 3. Cyclic voltammograms of compounds **3**–**6** in N,N-dimethylformamide (DMF) solution, versus Ag/Ag^+.

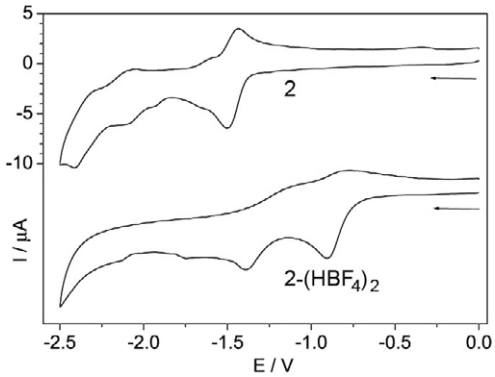

Figure 4. Cyclic voltammograms of the wire molecule **2** and its tetrafluoroborate salt in DMF solution, versus Ag/Ag^+.

wave for **4** at more negative potentials is presumably associated with reduction of the terminal ethynyls. Similar data have been observed for other ethynyl-fluorenone derivatives [29] and extended arylene-ethynylene oligomers incorporating fluorenone units [30].

The introduction of the pyridyl unit(s) led to significant changes in the cyclic voltammograms. Unlike the fluorene analogue **4**, both the reduction waves of **5** were irreversible. Predictably the C=C bond of the (4-pyridyl)methylene moiety of **5** is harder to reduce than the carbonyl of **4**, and the derived methylene radical anion is less stable, possibly undergoing side-reactions at the exocyclic methylene carbon. In contrast, the dipyridyl analogue **6** underwent two, fully-reversible, single-electron reductions (figure 3) to yield the stabilized dianion species $\mathbf{6}^{2-}$ (presumably comprising a fluorenyl anion and a dipyridylmethylene anion species). No further reduction waves were observed on scanning cathodically to −2.75 V (versus Ag/Ag^+). For the 7 nm wires **1** and **2** the redox behaviour is less clean at potentials more negative than about −1.6 V, where irreversible processes were observed. If the reductive scan was limited to −1.8 V the first wave was cleanly reversible for all the compounds. Protonation of the pyridyl moieties of **1**, **2** (figure 4) **5** and **6** with HCl or HBF_4 led to a new irreversible wave (about +500 to 600 mV compared to the neutral precursors) consistent with the one-electron reduction of the pyridinium moieties.

The improved stability of the 9-[di(4-pyridyl)methylene] fluorene units compared to the mono-pyridyl analogues

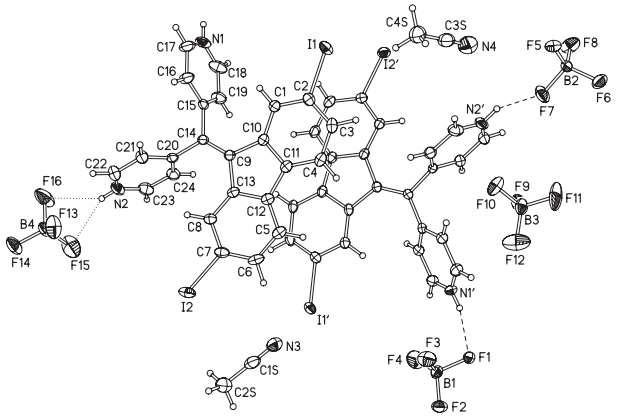

Figure 5. The asymmetric unit of **8**, showing 50% displacement ellipsoids and hydrogen bonds (dashed lines). The disorder of the tetrafluoroborate anions $B(1)F_4$ and $B(3)F_4$ is omitted for clarity.

(especially in the reduced states) prompted us to focus our attention on wire molecule **2**.

3.2. X-ray crystal structures of 7 and 8

The crystal structures of the model compound 2,7-diiodo-9-[di(4-pyridyl)methylene]fluorene **7** [28] and its dipyridinium salt **8** were obtained to shed light on the conformation adopted by the central core of the approximately 7 nm molecule **2** and its diprotonated salt (see section 5). The asymmetric unit of **8** comprises two dications $\mathbf{7}^{2+}$, four BF_4^- anions (two of them disordered) and two acetonitrile molecules of crystallization (figure 5). The dicationic nature of **8** was proved by the location (from difference Fourier analysis) and refinement of hydrogens at all N atoms, three of which form strong hydrogen bonds and one a weak (trifurcated) hydrogen bond N–H···F. The C–N–C bond angles in **8** are significantly wider than in neutral **7** (mean 122.7(3)° versus 116.7(2)°) as expected upon protonation. Bond distances in **7** and both dications of **8** are similar, with substantially double-bond character of the C(9)=C(14) bond (mean 1.351(3) Å in **8** versus 1.358(3) Å in neutral **7**). However, the molecular conformations are somewhat different (figure 6). The dication **8**A has an approximate local C_s symmetry with the *m* plane normal to the fluorene moiety. Both C(9) and C(14) atoms are slightly pyramidalized, deviating by 0.04 and 0.06 Å from ideal sp^2 planes, which form a dihedral angle of 4.6°. Thus the $C_2C(9)=C(14)C_2$ moiety has a boat-like distortion. The pyridinium rings are inclined by 81.9° and 84.7° to the plane of C(14). Dication **8**B is closer to C_2 symmetry, like neutral **7**. Both C(9) and C(14) atoms are practically planar while a twist around the C(9)=C(14) bond amounts to 13.2° (cf 10.8° in **7**). The pyridinium rings are rotated in the same direction (cf opposite directions in A), forming dihedral angles of 45.4° and 73.9° with the C(14) plane (in neutral **7**, 71.5° and 62.0°, respectively, for the pyridyl rings).

4. Self-assembled monolayers of 2

Removal of cyanoethyl protecting groups from aromatic thiols can be achieved under basic conditions [30]. Gold-

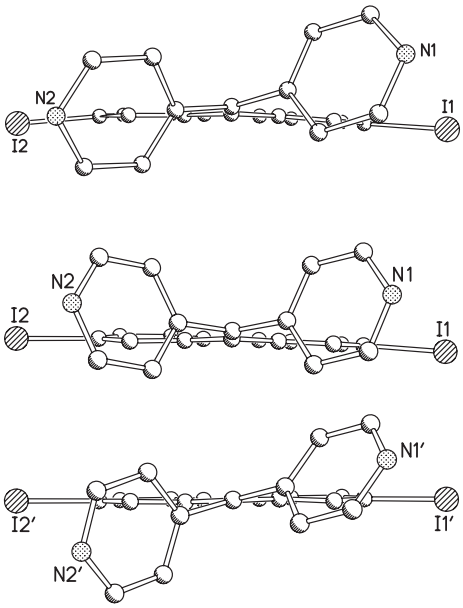

Figure 6. Conformations of the neutral molecule **7** (top) and its dications **8** A (middle) and **8** B (bottom), viewed down the C(9)=C(14) bond.

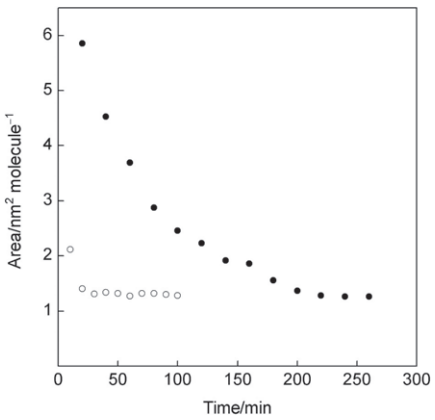

Figure 7. Variation of the molecular area with the period of immersion of a gold-coated 10 MHz quartz crystal in a tetrahydrofuran solution of **2** (filled circles) and to the same solution to which NaOMe was added to deprotect the thiolates (open circles).

coated substrates were immersed in a tetrahydrofuran solution of **2** containing sodium methoxide, and the formation of the self-assembled monolayer (SAM) was monitored from the frequency changes following deposition on gold-coated 10 MHz quartz crystals. The frequency saturated after about 0.5 h to a constant value of about 1.3 nm^2/molecule for the chemisorbed wire, based on a Sauerbrey analysis [31] of the data (figure 7). In the absence of sodium methoxide the time increased to about 4 h. The area is consistent with the calculated value from the van der Waals dimensions of the molecular wire, assuming partial overlap of the highly tilted molecules in the SAM.

Evidence of self-assembly of **2** was provided by x-ray photoelectron spectroscopy which revealed a doublet at 162.1 and 163.5 eV (S $2p_{3/2}$ and S $2p_{1/2}$) corresponding to the

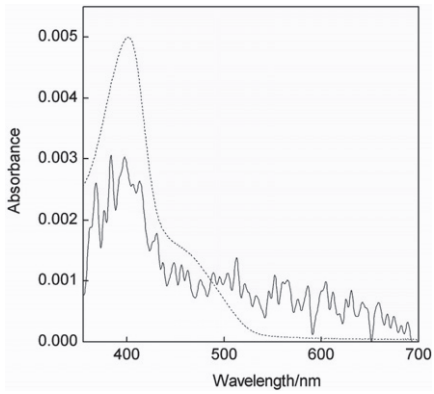

Figure 8. UV/visible absorption spectrum of SAMs of **2** on a platinum-coated glass slide (solid line) and the spectrum of **2** in tetrahydrofuran solution (dotted line).

binding energy of the gold thiolate link. Another doublet at 163.7 and 164.6 eV is characteristic of a surface-based terminal thiol group. The UV/visible spectrum of the SAM on platinum-coated glass exhibited a peak at λ_{max} about 400 nm when corrected for absorbance of the substrate, which is similar to the solution spectrum of **2** in chloroform (λ_{max} 400, 450 (shoulder) nm) (figure 8).

5. Electrical measurements

SAMs of **2** on gold-coated highly oriented pyrolytic graphite (HOPG) were analyzed using STM techniques. Symmetrical I–V characteristics were observed, as expected from symmetrical wire-like molecules located between gold contacts (figure 9). The set-point current and voltage had very little effect on the profile of the I–V curves but they did affect the magnitude of the tunnelling current by influencing the distance between the probe and the surface. This is a common feature from STM studies on wire-like molecules in this series, e.g. molecule **1** [32].

The dipyridyl functionality of wire molecule **2** has been utilized to obtain a rectifying junction in which the cationic wire is the electron-accepting component in combination with an adjacent anionic electron-donating layer. To achieve this the self-assembled wire was diprotonated to form the $[Au–\mathbf{2}H_2^{2+}(Cl^-)_2]$ salt; the counterions were then exchanged using a solution of tetrasodium copper phthalocyanine-3,4′,4″,4‴-tetrasulfonate to provide a bilayer assembly of the composition $Au\text{-}\mathbf{2}H_2^{2+}[CuPc(SO_3^-)_4(Na^+)_n]_{2/(4-n)}$. The process was monitored from the frequency of 10 MHz quartz crystals, which saturated after about 70 min, and a Sauerbrey analysis of the frequency change provided an area of about 0.8 nm^2/molecule for the negatively charged phthalocyanine. This area is consistent with the molecules standing on edge and comparison with data obtained for the initially formed SAM yielded a wire to $CuPc(SO_3^-)_4(Na^+)_n$ ratio of about 1:1.6. It should be noted that based on the x-ray crystal structures shown in figure 6, no significant changes in the conformation of the wire will have resulted from the diprotonation.

Bilayers formed by this method were investigated by both x-ray photoelectron and visible spectroscopy and provide evidence of the ionic exchange. For example, an XPS

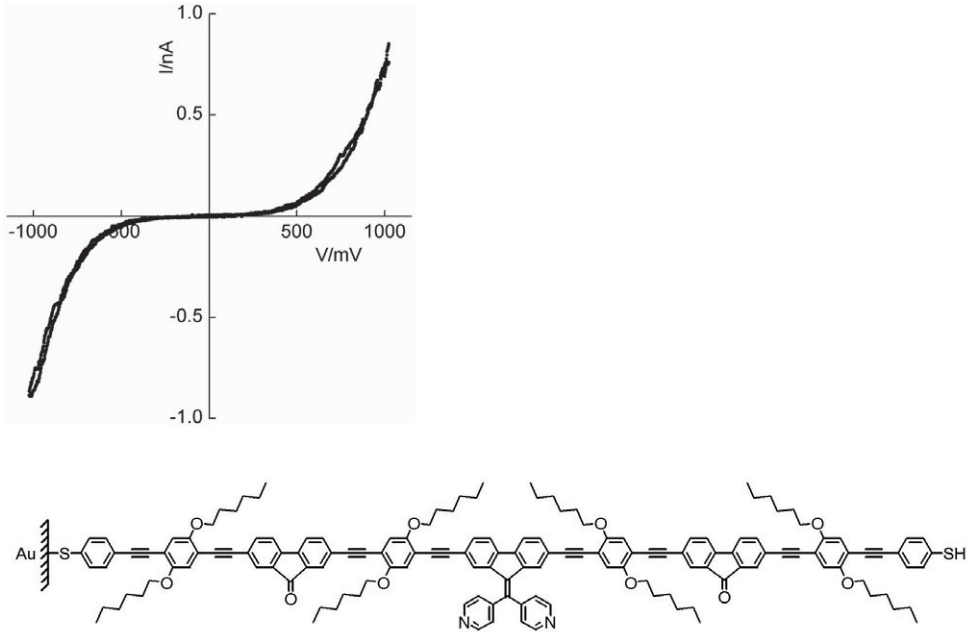

Figure 9. Symmetrical I–V characteristics of **2** deposited as a SAM on gold-coated HOPG and contacted by a gold probe for set-point current and sample bias of 0.3 nA and 30 mV, respectively. The designated polarity relates to the substrate electrode. The assembled structure of the deprotected wire **2** is shown.

peak at 935 eV (Cu 2p) corresponds to the binding energy of a metal atom unique to the phthalocyanine counterion and a broad transition at λ_{max} about 700 nm, attributed to its Q band, is in a region where the wire is transparent. Most importantly, the I–V characteristics were reproducibly different. As expected, the diprotonated wire with chloride counterions [Au–**2**$H^{2+}(Cl^{-})_2$] exhibited symmetrical I–V characteristics (like the neutral wire in figure 9), whereas the bilayer film with phthalocyanine counterions exhibited rectifying curves with current ratios of 20–40 at ± 1 V (figure 10). These arise from the designated donor/acceptor sequence whereby the favourable direction of electron flow is from the substrate to electron-accepting molecular wire and from the electron-donating phthalocyanine to the probe. In this direction, the substrate and probe are cathode and anode respectively and, when these are reversed, there is an energy mismatch between the molecular orbitals and the Fermi levels of the contacting electrodes which gives rise to the rectifying behaviour. Moreover, at forward bias, the observed current is significantly higher than for the wire alone, and this probably results from the more closely aligned energies of the Fermi levels with the highest occupied and lowest unoccupied molecular orbitals of the donor and acceptor, respectively.

6. Theoretical studies

An *ab initio* approach, using a combination of the density-functional theory (DFT) code SIESTA [33] and a Green's function scattering approach, as encapsulated in the non-equilibrium molecular electronics SMEAGOL code [34], was used to calculate the electron transport properties of the molecular wires **1** and **2** (with methoxy side groups replacing the hexyloxy side chains). This simplification has been shown to have little effect on the computed conductance [35]. To describe charge transfer effects at the lead–molecule surface, the molecules were then extended to include the surface layers of gold leads, with semi-infinite leads then seamlessly attached via Dyson's equation. Due to the large size of these molecules we focused on the conductance at zero bias.

The transmission coefficient $T(E)$ for wire **1** with a central 9-[(4-pyridyl)methylene]fluorene moiety shows a variety of resonant features about the Fermi energy ($E_F = 0$ eV) (figure 11). The LUMO resonances at $E \sim 1$ eV show typical Lorentzian line shapes corresponding to Breit–Wigner resonances through the molecular levels delocalized across the backbone of the wire; because the molecule is symmetric the magnitude of these resonances is unity. Closer to the Fermi energy $E \sim 0.1$ eV we find three resonances followed by three antiresonances, with shapes typical of asymmetric Fano resonances [36].

To demonstrate that these are associated with quasi-bound states located on the side groups attached to the molecule, figure 11 also shows the transmission coefficient through the molecular wire **2** which contains a central 9-[di(4-pyridyl)methylene]fluorene moiety. In this case the three Fano resonances have shifted to lower energy, causing the zero-bias conductance to decrease by three orders of magnitude. Figure 12 shows that this sensitivity to the character of the side group is also reflected in the energy levels of the isolated molecular wires. For molecule **1** the HOMO–LUMO gap is much larger than that of molecule **2** and also the three LUMO resonances are more spread. In molecule **2** the LUMO resonances consist of two levels close together, with one further away. The same pattern is present in the transmission data.

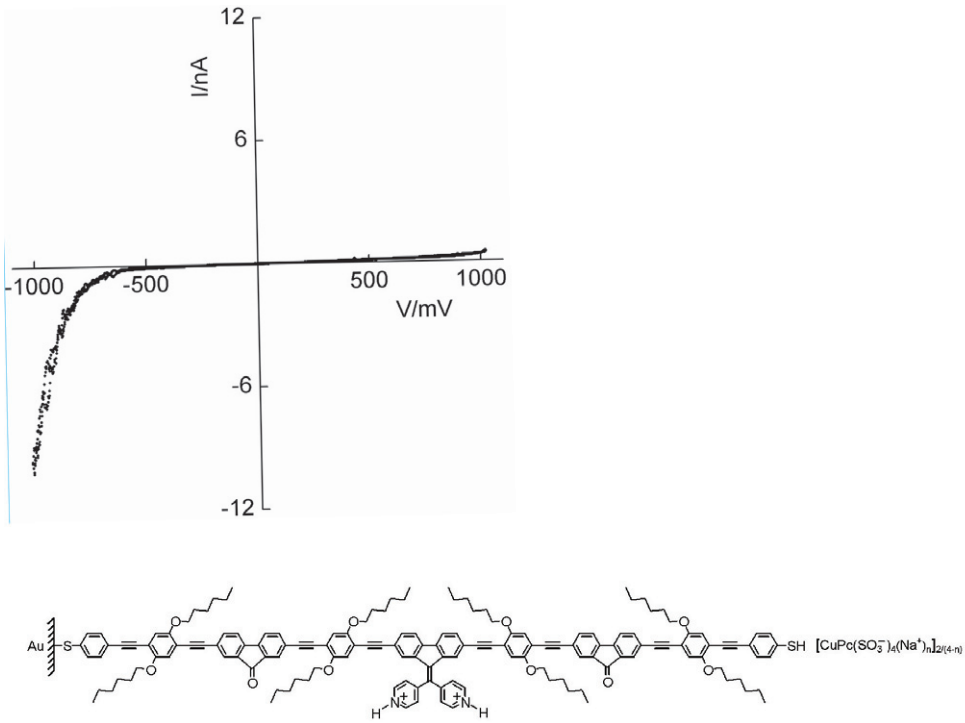

Figure 10. Rectifying I–V characteristics of the Au–$\mathbf{2}H_2^{2+}[CuPc(SO_3^-)_4(Na^+)_n]_{2/(4-n)}$ bilayer assembly contacted by a gold probe for set-point current and sample bias of 0.8 nA and 35 mV, respectively. The designated polarity relates to the substrate electrode. The assembled structure of the diprotonated wire ionically coupled in the bilayer is shown.

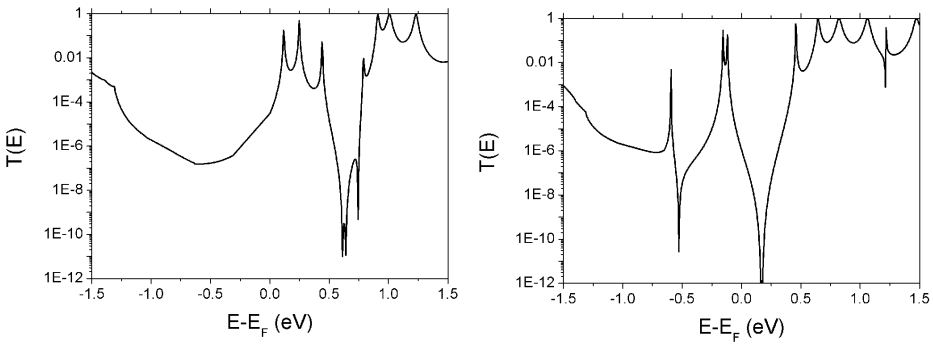

Figure 11. Zero-bias transmission through the 7 nm wires **1** (left) and **2** (right).

The results shown in figures 11 and 12 suggest that these molecular wires possess useful structural features which allow the conductance of the molecule to be altered by changing the properties of the side groups attached to the fluorene backbone units. This opens up the possibility of using such structures for sensing.

7. Conclusions

A variety of techniques have shown that diprotonation of the dipyridyl functionality of the 7 nm long molecule **2** can be harnessed to tune the electronic properties of the wire. Cyclic voltammetric data established that fluorenone and 9-[di(4-pyridyl)methylene]fluorene units in **2** are suitable electron acceptor components for n-dopable molecular wire structures, whereas 9-[(4-pyridyl)methylene]fluorene appears to be less suitable due to its irreversible electrochemical reduction properties. The striking difference in the I–V characteristics of SAMs of the non-protonated wire Au–**2** and the ionic Au–$\mathbf{2}H_2^{2+}[CuPc(SO_3^-)_4(Na^+)_n]_{2/(4-n)}$ bilayer assembly (symmetrical I–V characteristics, and rectifying behaviour, respectively) in STM experiments conclusively proves the presence of the wire molecules in the junction. Single-molecule studies will be reported separately [37]. Additionally, we will explore the fascinating prospect that these arrays could function as a platform for chemical sensing where conduction along the wire backbone could be modulated by a binding event at pendant receptor sites.

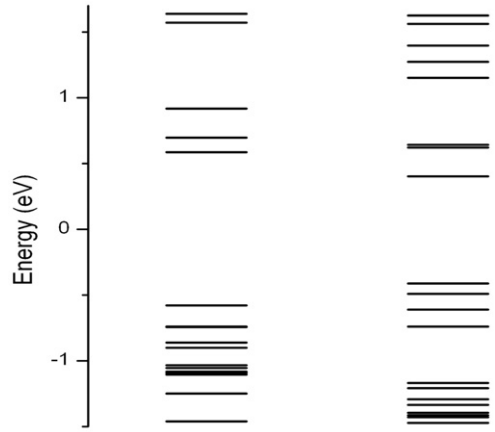

Figure 12. Calculated energy levels of the isolated molecular wires **1** (left) and **2** (right).

8. Experimental details

*8.1. Synthesis of 2,7-diiodo-9-[bis(4-pyridinium)methylene] fluorene bis(tetrafluoroborate) salt **8***

To a solution of **7** [22] in 1,4-dioxane was added dropwise tetrafluoroboric acid diethyl ether complex (Aldrich, 85%) until precipitation was complete. The mixture was vacuum evaporated to dryness to afford an orange solid of **8**. The solid was dissolved in acetonitrile followed by the slow addition of toluene, leading to the gradual precipitation of an orange solid. The solid suspension was heated to boiling then cooled slowly, yielding orange single crystals for x-ray structure analysis.

8.2. Electrochemical studies

The general procedures have been reported previously [28]. Cyclic voltammograms were recorded using a BAS CV50W electrochemical analyser and the potentials quoted were referenced to Ag/Ag^+ non-aqueous reference electrode, which contains a solution of 0.01 M $AgNO_3$ and 0.1 M $TBAPF_6$ in acetonitrile. A Pt disk (diameter = 1.6 mm) was used as the working electrode and a Pt wire was used as counterelectrode. In all cases, the potentials were scanned at 100 mV s^{-1}.

8.3. Self-assembly

Monolayers of **2** were formed by immersing gold-coated substrates in a tetrahydrofuran solution of **2** (0.1 mg ml^{-1}) to which sodium methoxide in methanol was added to facilitate removal of the protecting groups. The SAMs were thoroughly rinsed with tetrahydrofuran to remove physisorbed material. Exposure of the SAM to HCl vapour gave the [Au–$\mathbf{2}H_2^{2+}(Cl^-)_2$] salt, and then the chloride counterions were exchanged by immersion in an aqueous methanol solution of tetra sodium copper phthalocyanine-3,4′,4″,4‴-tetrasulfonate, followed by thorough rinsing of the SAM with water to remove NaCl from the lattice to give Au–$\mathbf{2}H_2^{2+}[CuPc(SO_3^-)_4(Na^+)_n]_{2/(4-n)}$.

8.4. Electrical characterization

SAMs of **2** were investigated using a MultiMode scanning tunnelling microscope with a Nanoscope IV controller (Veeco Instruments, Cambridge). For I–V characterization, the gold probe was landed at distinct surface features distant from grain boundaries. In each case, the SAMs were investigated at several locations across the surface and the I–V data were averaged from multiple scans at each of these sites.

8.5. Theoretical studies

Initially, to find the optimum geometry, the isolated molecules were relaxed using SIESTA until all the force components on the atoms were smaller than 0.02 eV $Å^{-1}$. To reduce the computational overhead, the hexyloxy side chains were substituted by methoxy groups. To describe charge transfer effects at the lead–molecule surface, the molecules were then extended to include the surface layers of gold leads. Semi-infinite leads were then seamlessly attached via Dyson's equation. Using double-zeta plus polarization orbitals, Troullier–Martins [38] pseudopotentials and the Ceperley–Alder [39] local density approximation (LDA) to describe the exchange correlation the zero-bias mean field Hamiltonian of the extended molecule was calculated. Finally the scattering matrix and transmission coefficient $T(E)$ were computed and the zero-bias electrical conductance is given by the Landauer formula $G = (2e^2/h)T(E_F)$, where E_F is the Fermi energy [40].

8.6. X-ray crystal data

Data collection: Siemens SMART three-circle diffractometer with a SMART 1 K CCD area detector, Mo Kα radiation, graphite monochromator, $\bar{\lambda}$ = 0.710 73 Å. The structure was solved by direct methods and refined by full-matrix least squares against F^2 of all reflections, using SHELXTL software [41]. *Crystal data*: **8** $(C_{24}H_{16}N_2I_2^{2+})(BF_4^-)_2{\cdot}MeCN$, M = 800.86, T = 120 K, triclinic, space group $P\bar{1}$ (No. 2), a = 13.073(2), b = 14.084(2), c = 17.150(2) Å, α = 72.58(1), β = 73.36(1), γ = 82.13(1)°, U = 2882.2(7) $Å^3$, Z = 4, D_c = 1.846 g cm^{-3}, μ = 2.26 mm^{-1}, 40 117 reflections ($2\theta \leqslant 58°$), 15 253 unique, R_{int} = 0.069 (0.024 after a semi-empirical absorption correction based on Laue equivalents [42]), R = 0.025 on 13 034 unique data with $F^2 \geqslant 2\sigma(F^2)$, $wR(F^2)$ = 0.058 on all data. The full data have been deposited at the Cambridge Crystallographic Data Centre: CCDC-615717. The data for **7** have been reported previously [28].

Acknowledgments

We thank the EPSRC and QinetiQ for supporting the work at Durham, Cranfield and Lancaster. The work at Cranfield was additionally supported by the Department of Trade and Industry and the Royal Society/Wolfson Foundation.

References

[1] Lundstrom M 2003 *Science* **299** 210
[2] Petty M C, Bryce M R and Bloor D (ed) 1995 *An Introduction to Molecular Electronics* (Oxford: Oxford University Press)

[3] Nitzan A and Ratner M A 2003 *Science* **300** 1384
[4] Heath J R and Ratner M A 2003 *Phys. Today* **56** 43
[5] Maruccio G, Cingolani R and Rinaldi R 2004 *J. Mater. Chem.* **14** 542
[6] Wassel R A and Gorman C B 2004 *Angew. Chem. Int. Edn* **43** 5120
[7] Ashwell G J, Urasinska B and Tyrrell W D 2006 *Phys. Chem. Chem. Phys.* **8** 3314
[8] Robertson N and McGowan C A 2003 *Chem. Soc. Rev.* **32** 96
[9] Benniston A C 2004 *Chem. Soc. Rev.* **33** 573
[10] Joachim C, Gimewski J K and Aviram A 2000 *Nature* **408** 541
[11] James D K and Tour J M 2004 *Chem. Mater.* **16** 4423
[12] McCreery R L 2004 *Chem. Mater.* **16** 4477
[13] Joachim C and Ratner M A 2004 *Nanotechnology* **15** 1065
[14] Grüter L, Cheng F, Heikkilä T T, González M T, Diederich F, Schönenberger C and Calame M 2005 *Nanotechnology* **16** 2143
[15] Tour J M *et al* 2001 *Chem. Eur. J.* **7** 5118
[16] Wei L, Padmaja K, Youngblood W J, Lysenko A B, Lindsey J S and Bocian D 2004 *J. Org. Chem.* **69** 1461
[17] Zhitenev N B, Erbe A, Meng H and Bao Z 2003 *Nanotechnology* **14** 254
[18] Kushmerick J G, Wjitaker C M, Pollack S K, Schull T L and Shashidhar R 2004 *Nanotechnology* **15** S489
[19] Bunz U H F 2000 *Chem. Rev.* **100** 1065
[20] Tour J M 2000 *Acc. Chem. Res.* **33** 791
[21] Atienza C, Insuasty B, Seoane C, Martín N, Ramey J, Rahman G M A and Guldi D M 2005 *J. Mater. Chem.* **15** 124
[22] Wang C, Batsanov A S and Bryce M R 2006 *J. Org. Chem.* **71** 108
[23] James P V, Sudeep P K, Suresh C H and Thomas K G 2006 *J. Phys. Chem.* A **110** 4329
[24] Seminario J M, Zacarias A G and Tour J M 2000 *J. Am. Chem. Soc.* **122** 1964
[25] Chen J, Wang W, Reed M A, Rawlett A M, Price D W and Tour J M 2000 *Appl. Phys. Lett.* **77** 1224
[26] Tour J M, Cheng L, Nackashi D P, Yao Y, Flatt A K, St Angelo S K, Mallouk T E and Franzon P D 2003 *J. Am. Chem. Soc.* **125** 13279
[27] Haiss W, Wang C, Grace I, Batsanov A S, Schiffrin D J, Higgins S J, Bryce M R, Lambert C J and Nichols R J 2006 *Nature* accepted
[28] Wang C, Batsanov A S and Bryce M R 2006 *Faraday Discuss.* **131** 221
[29] Price D W Jr and Tour J M 2003 *Tetrahedron* **59** 3131
[30] Wang C, Batsanov A S, Bryce M R and Sage I 2004 *Org. Lett.* **6** 2181
[31] Sauerbrey G 1959 *Z. Phys.* **155** 206
[32] Ashwell G J, Tyrrell W D, Urasinska B, Wang C and Bryce M R 2006 *Chem. Commun.* 1640
[33] Soler J M, Artacho E, Gale J D, Garcia A, Junquera J, Ordejon P and Sanchez-Portal D 2002 *J. Phys.: Condens. Matter* **14** 2745
[34] Rocha A R, Garcia-Suarez V, Bailey S W, Lambert C J, Ferrer F and Sanvito S 2006 *Phys. Rev.* B **73** 085414
[35] Grace I M, Bailey S W, Jefferson J and Lambert C J 2004 *Mater. Sci. (Poland)* **22** 507
[36] Fano U 1961 *Phys. Rev.* **124** 1866
[37] Ashwell G J, Urasinska B, Wang C, Bryce M R, Grace I and Lambert C J 2006 *Chem. Comm.* 4706–8
[38] Troullier N and Martins J L 1991 *Phys. Rev.* B **43** 1993
[39] Zunger A and Perdew J P 1981 *Phys. Rev.* B **23** 5048
[40] Büttiker M, Imry Y, Landauer R and Pinhas S 1985 *Phys. Rev.* B **31** 6207
[41] Sheldrick G M 2003 *SHELXTL Version 6.14* (Madison, WI: Bruker AXS)
[42] Sheldrick G M 2003 *SADABS 2.10* (Madison, WI: Bruker AXS)